fluctuational paths. The relaxational tail leading back to the stable state S is common to the two fluctuational paths that form the resultant corral[12]. From Fig. 2c we see that the ridges of the distribution are strongly asymmetric in time, but agree well with the fluctuational and relaxational paths predicted from equations (3). The observed asymmetry of the distribution implies[4] a lack of detailed balance; and it leads directly[15,26] to macroscopic irreversibility in the $D \rightarrow 0$ limit where the width of the distribution tends to zero. In verifying the existence of the switching line, the results demonstrate the non-differentiability of the generalized nonequilibrium potential.

One third example (Fig. 3) is the system suggested by Maier and Stein[19,26] for analysis of the escape problem in nonequilibrium systems. It consists of a bistable system driven from equilibrium by a stationary field of (in general) the nongradient type. In measurements near one of the stable states, the lack of detailed balance and the irreversibility of the fluctuations become strikingly apparent. Figure 3a shows the measured $P_f(x,y)$ distribution for fluctuations to the two different remote states $\mathbf{x}_f$ placed symmetrically on either side of the y axis; $P_f(x,y)$ is the projection of $P_f(x_i,y_i,t_i;\ x,y,t;\ x_f,y_f,t_f)$ onto the x–y plane with $t_f = 0$ as before. When the paths traced out by the ridges are plotted (Fig. 3b), it can be seen: (1) that the fluctuational trajectories are completely different from the relaxational ones; and (2) that they are in good agreement with the fluctuational and relaxational trajectories predicted from equations (3). Figure 3c shows the corresponding picture measured for fluctuations to a single remote state $\mathbf{x}_f$ on the switching line (lying on the x axis). The two fluctuational paths to the remote state are, again, markedly different from the common relaxational path leading back to S. Both parts of the trajectory are well described by the corresponding optimal paths calculated from equations (3). In this case too, therefore, the observations link a lack of detailed balance to macroscopic irreversibility, and demonstrate the nondifferentiability of the generalized nonequilibrium potential; the closed loops traversed during fluctuations verify the expected[2,26,27] occurrence of rotational flow in nonequilibrium systems.

Thus, after more than 60 years of "thought experiments" on large fluctuations[2,3,30], it has now become possible to do real experiments yielding quantitative results. Our work has already verified several long-standing theoretical predictions, including those of symmetry between the growth and decay of classical fluctuations in equilibrium[2,30], the breaking of this symmetry under nonequilibrium conditions[7,15,26], the relationship of symmetry-breaking to a lack of detailed balance[15–17,26], and the existence of an optimal force derived from the fluctuating field and related to the momentum of an auxiliary hamiltonian system[8–10,20,21]. The technique has also enabled us to reveal new dynamical features of large fluctuations, such as critical broadening of the prehistory probability distribution[12]. It will be as applicable to future experiments on natural systems as it has been to the electronic models studied here. Because equations (1) can, at least in some cases[9,31], be related directly to the microscopic classical equations of motion for a system interacting with a heat bath, the approach illuminates connections between microscopic reversibility and macroscopic irreversibility. Other open questions needing urgently to be addressed include the precise physical meaning of the momentum $\mathbf{p}$ and the role of entropy and how it changes during fluctuational motion. □

Received 7 January; accepted 23 July 1997.

1. Einstein, A. Über die von der molekularkinetischen Theorie der Wärme geforderte Bewegung von in ruhenden Flüssigkeiten Suspendierten Teilchen. *Ann. Phys.* **17,** 549–560 (1905); also transl. in *Investigations on the Theory of the Brownian Movement* (ed. Fürth, R.) (Dover, New York, 1956).
2. Onsager, L. Reciprocal relations in irreversible processes. I. *Phys. Rev.* **37,** 405–426 (1931).
3. Landau, L. D. & Lifshitz, E. M. *Statistical Physics* Part 1, 3rd edn (Pergamon, New York, 1980).
4. Schulman, L. S. Models for intermediate time dynamics with two-time boundary conditions. *Physica A* **117,** 373–380 (1991).
5. Bricmont, J. Science of chaos or chaos in science? *Ann. NY Acad. Sci.* **775,** 131–175 (1996).
6. Cohen, J. K. & Lewis, R. M. A ray method for the asymptotic solution of the diffusion equation. *J. Inst. Math. Appl.* **3,** 266–290 (1967).
7. Freidlin, M. I. & Wentzell, A. D. *Random Pertubations in Dynamical Systems* (Springer, New York, 1984).
8. Feynman, R. P. & Hibbs, A. R. *Quantum Mechanics and Path Integrals* (McGraw-Hill, New York, 1965).
9. Dykman, M. I. & Krivoglaz, M. A. in *Soviet Physics Reviews* Vol. 5 (ed. Khalatnikov, I. M.) 265–441 (Harwood, New York, 1984).
10. Bray, A. J. & McKane, A. J. Instanton calculation of the escape rate for activation over a potential barrier driven by colored noise. *Phys. Rev. Lett.* **62,** 493–496 (1989).
11. Dykman, M. I., McLintock, P. V. E., Smelyanskiy, V. N., Stein, N. D. & Stocks, N. G. Optimal paths and the prehistory problem for large fluctuations in noise-driven systems. *Phys. Rev. Lett.* **68,** 2718–2721 (1992).
12. Dykman, M. I., Luchinsky, D. G., McClintock, P. V. E. & Smelyanskiy, V. N. Corrals and critical behaviour of the distribution of optimal paths. *Phys. Rev. Lett.* **77,** 5229–5232 (1996).
13. Kautz, R. L. Noise, chaos, and the Josephson standard. *Rep. Prog. Phys.* **59,** 935–992 (1996).
14. Dykman, M. I. *et al.* Noise-enhanced optical heterodyning. *Appl. Phys. Lett.* **67,** 308–310 (1995).
15. Dykman, M. I., Mori, E., Ross, J. & Hunt, P. M. Large fluctuations and optimal paths in chemical kinetics. *J. Chem. Phys.* **100,** 5737–5750 (1994).
16. Graham, R. & Tél, T. Existence of a potential for dissipative dynamical systems. *Phys. Rev. Lett.* **52,** 9–12 (1984).
17. Graham, R. in *Noise in Nonlinear Dynamical Systems* Vol. 1 (eds Moss, F. & McClintock, P. V. E.) 225–278 (Cambridge Univ. Press, 1989).
18. Dykman, M. I., Millonas, M. M. & Smelyanskiy, V. N. Observable and hidden features of large fluctuations in nonequilibrium systems. *Phys. Lett. A* **195,** 53–58 (1994).
19. Maier, R. S. & Stein, D. L. A scaling theory of bifurcations in the symmetrical weak-noise escape problem. *J. Statist. Phys.* **83,** 291–357 (1996).
20. Dykman, M. I. Large fluctuations and fluctuational transitions in systems driven by colored Gaussian noise—a high-frequency noise. *Phys. Rev. A* **42,** 2020–2029 (1990).
21. Einchcomb, S. J. B. & McKane, A. J. Use of Hamiltonian mechanics in systems driven by colored noise. *Phys. Rev. E* **51,** 2974–2981 (1995).
22. Van Kampen, N. G. *Stochastic Processes in Physics and Chemistry* (Elsevier, Amsterdam, 1990).
23. Berry, M. V. Waves and Thom's theorem. *Adv. Phys.* **25,** 1–26 (1976).
24. Jauslin, H. R. Nondifferentiable potentials for nonequilibrium steady states. *Physica A* **144,** 179–191 (1987).
25. Day, M. V. Recent progress on the small parameter exit problem. *Schochastics* **20,** 121–150 (1987).
26. Maier, R. S. & Stein, DS. L. Escape problem for irreversible systems. *Phys. Rev. E* **48,** 931–938 (1993).
27. Risken, H. *The Fokker-Planck Equation* 2nd edn (Springer, Berlin, 1989).
28. McClintock, P. V. E. & Moss, F. in *Noise in Nonlinear Dynamical Systems* Vol. 3 (eds Moss, F. & McClintock, P. V. E.) 243–274 (Cambridge Univ. Press, 1989).
29. Haken, H. Cooperative phenomena in systems far from thermal equilibrium and in nonphysical systems. *Rev. Mod. Phys.* **47,** 67–119 (1975).
30. Onsager, L. & Machlup, S. Fluctuations and irreversible processes. *Phys. Rev.* **91,** 1505–1512 (1953).
31. Zwanzig, R. Nonlinear generalised Langevin equations. *J. Statist. Phys.* **9,** 215–220 (1973).

Acknowledgements. We thank M. I. Dykman for help and encouragement; we also thank him, R. S. Maier and D. L. Stein for comments on an earlier version of the manuscript; and we acknowledge correspondence with N. G. van Kampen. This work was supported by the Engineering and Physical Sciences Research Council (UK), the Royal Society, and the Russian Foundation for Basic Research.

Correspondence should be addressed to P.V.E.MC. (e-mail: p.v.e.mcclintock@lancaster.ac.uk).

Light amplification in organic thin films using cascade energy transfer

M. Berggren, A. Dodabalapur, R. E. Slusher & Z. Bao

Bell Laboratories, Lucent Technologies, 600 Mountain Avenue, Murray Hill, New Jersey 07974, USA

There is currently renewed interest in the development of lasers using solid-state organic and polymeric materials as the gain media. These materials have a number of properties that make them good candidates for such applications—for example, emission bands that are displaced (via a Stokes shift) from absorption bands, and the ease with which the emitting species can be embedded in a suitable host material[1–5]. But despite these advantages, the threshold power densities required for light amplification that have been reported so far have been high[6–8]. Here we describe an approach, based on energy transfer between molecular species, that can lower the threshold for stimulated emission and laser action while improving markedly the waveguiding properties of the active material. In our materials, an initial molecular excited state is generated in the host compound by absorption of light; this state is then resonantly and non-radiatively transferred down in energy (through one or more steps)

between suitably matched dye molecules dispersed in the host, so ensuring that the absorption losses at the final emission wavelengths are very small. Such composite gain media provide provide broad tunability of the emission wavelength, and also decouple the optical emission properties from the transport properties, so providing greater flexibility for the design of future electrically driven device structures.

Solid-state lasers based on organic materials, with a few recent exceptions, have had gain media consisting of a suitable transparent host doped with a small percentage of dye[2–5]. In such media there is no significant optical interaction between the host molecules and the dye molecules; the host serves mainly to physically separate the fluorescent dye molecules, which has the beneficial effect of hindering concentration quenching[1], and increasing the quantum yield of the material. As the host matrix is non-absorbing, and the volume fraction of the emissive dye is small (of the order of 1%), the amount of incident light that can be absorbed in a film of thickness ~150–200 nm (a typical value for the thickness that supports only the lowest-order optical mode) is very small (<5%). This places a lower limit on the threshold power density necessary to have stimulated emission.

One way to circumvent this limit is to have a host material which has optical gain. There have been several recent examples of such luminescence in conjugated polymers[6–8]. It is also possible to obtain stimulated emission in pure films of small molecules, an example of which will be given below. Although the absorption of incident light can be high in such materials, the absorption losses at the emission wavelengths can be quite high ($>1\,cm^{-1}$). This is because the absorption coefficient is quite high in most organic materials close to the absorption 'edge', and it is necessary to shift the luminescence (sometimes by >200 nm) from this edge to significantly lower the absorbance. A low absorbance at the emission wavelength(s) will mean that the optical gain and minimum pump power necessary for population inversion is lowered. One way to accomplish this is to use gain media with energy transfer[9,10]. In the most general case, the energy transfer can take place through multiple steps, a process we call cascade energy transfer. This process requires three or more materials which have absorption and emission spectra that suitably matched. We believe that this report represents the first time cascade energy transfer has been used in an optical device. Single-step energy transfer can also be useful in laser gain media, and we give some examples of this later.

In the materials studied here, light is absorbed by host material such as 2-(4-biphenylyl)-5-(4-*t*-butylphenyl)-1,3,4-oxadiazole (PBD) which is doped with a small percentage (of the order of 1 wt%) of one or more fluorescent dyes with different absorption and emission spectra. The function of the host is to absorb the pump light and funnel the excitation to the dye molecules through a Förster-type energy transfer. Because the average spacing between the dye molecules at the doping concentrations we use (3 nm) is less than the Förster distance[10], excitation transfer can be extremely efficient, especially if the overlap between the donor (host) emission spectrum and acceptor (dye) absorption spectrum is good. The absorption and emission spectra of the materials used are shown in Fig. 1. The spectra for PBD are from a pure film whereas the other spectra have been obtained from solid solutions of the dye in polystyrene. Efficient transfer was observed between PBD and coumarin 490 (C490) and between PBD and DCMII (with C490 included) and between PBD and LDS821 (with both C490 and DCMII also included in the film). (The dyes DCMII and LDS821 were obtained from Exciton, Inc., Dayton, Ohio). The transfer was poor between PBD and LDS821 when the intermediate dyes—C490 and DCMII—were not included in the film. These results are consistent with the predictions of resonance energy transfer theory[9,10]. To minimize the effects of reabsorption and almost eliminate waveguiding, the films were very thin and were deposited on aluminium. In other experiments, the relative quantum yield of films of the various materials were estimated relative to the quantum yield of a neat film of PBD (taken as 1). The quantum yields measured are 1.67 (PCD + C490), 1.49 (PCD + C490+ DCMII) and 0.6 (PBD + C490 + DCMII + LDS821).

The films that we used to study stimulated emission were deposited on glass substrates. The host material in the first set of studies was PBD which, together with any dopants, was deposited by spin-coating to form ~200-nm-thick films. The thickness of the films is such that only the lowest-order mode is guided by the planar waveguide formed by the PBD (core) and air and glass (cladding) layers. These films were photopumped with unfocused light from a pulsed nitrogen laser (wavelength $\lambda = 337$ nm) which emits 2-ns-long pulses with an energy density of 500 $\mu J\,cm^{-2}$ (corresponding to 250 $kW\,cm^{-2}$). The spot size was 3 mm × 2.5 cm. Neutral-density filters were used to adjust the pump power level. At low pump powers, the emission spectra are identical to the spontaneous emission spectra shown in Fig. 1. At sufficiently high pump powers the emission spectrum becomes narrower; such a narrowing is characteristic of amplification of spontaneous emission (ASE)

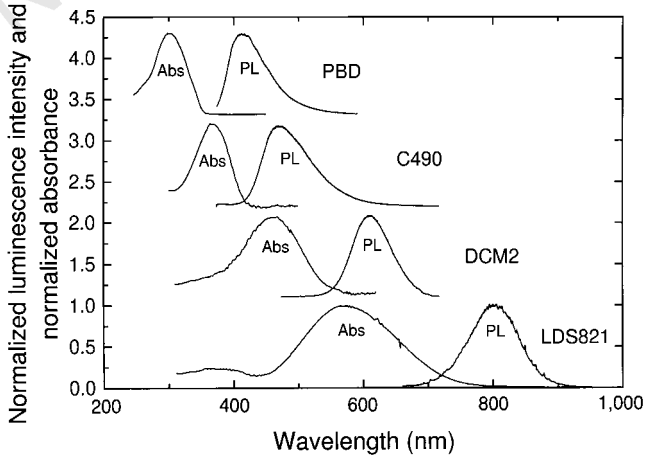

Figure 1 Absorbance and photoluminescence spectra of the host material and the fluorescent dyes. The host material is 2-(4-biphenylyl)-5-(4-*t*-butylphenyl)-1,3,4-oxadiazole (PBD); the dyes are coumarin 490 (C490), DCMII and LDS821. The spectra for PBD are from a pure film whereas the other spectra are from solid solutions of the material in polystyrene.

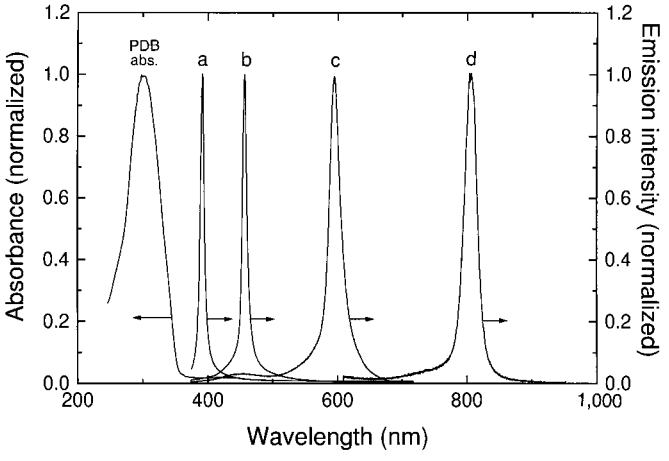

Figure 2 Normalized absorbance of PBD, and stimulated emission spectra from this material alone, and when doped with dyes. Curve a, PBD only; curve b, 0.6% C490 in PBD; curve c, 0.6% C490 + 0.9% DCMII in PBD; curve d, 0.6% C490 + 0.9% DCMII + 0.6% LDS821 in PBD.

and is observed in a wide variety of gain media. Films of undoped PBD also have such amplifying characteristics, as shown in Fig. 2 curve a. The threshold pump power (with a gain area of 3 mm × 2.5 cm) necessary to detect significant stimulated emission is ~10 kW cm^{-2}. One reason for this high value is that the peak of the ASE is close to the absorption 'edge' of the PBD where the absorption coefficient is high. As the gain coefficient has to be more than the absorption coefficient to have amplification, it follows that the pump power is necessarily high. Also shown in Fig. 2 are the ASE spectra (when pumped at 250 kW cm^{-2}) of PBD doped with 0.6% C490 (curve b) and 0.6% C490 + 0.9% DCMII (curve c). The peak of curve b which is at ~460 nm coincides almost exactly with the peak of the C490 spontaneous emission spectrum. The spontaneous emission from PBD at 460 nm is quite weak and separate measurements showed that energy transfer from PBD to C490 is very efficient. Thus, we attribute the ASE peak at 460 nm as due primarily to amplification of spontaneous emission from C490 following energy transfer from PBD. Similarly, in curve c the ASE peak is almost exclusively from DCMII as both PBD and C490 have very little or no spontaneous emission intensities at wavelengths near 600 nm. We found that energy transfer between PBD and DCMII was not as efficient as between PBD and C490 or between C490 and DCMII. Cascade energy transfer from PBD to DCMII via C490 molecules is the most likely pathway for excitation transfer. When the third dye (LDS821) was also included in the films, ASE centred near 805 nm was observed (curve d). The excitation transfer from PBD to LDS821 must proceed through one or more intermediate steps, as direct transfer from PBD to LDS821 is extremely inefficient. Based on studies of spontaneous emission in such doped films, we feel that the most likely pathway of excitation transfer is through both C490 and DCMII although two step transfers (through either C490 or DCMII) are also possible.

Figure 2 shows that pumping at 337 nm has resulted in a series of ASE peaks from the ultraviolet (392 nm) to the near infrared (805 nm). The thresholds for stimulated emission are the lowest for cases b, c and d where powers of 0.8–1.2 kW cm^{-2} are needed as opposed to 10 kW cm^{-2} for the pure film. As mentioned above, the chief reason for this is that the absorption coefficient is relatively low at wavelengths corresponding to peaks b, c and d.

We have fabricated distributed Bragg reflector lasers by pre-patterning a thermally oxidized Si wafer so as to form two gratings separated by distances in the range 3 mm to 1 cm. The gratings act as wavelength-selective mirrors. The grating period is 0.6 μm which results in reflectivity peaks near 610 nm, 485 nm and 392 nm, corresponding to the third, fourth and fifth orders, respectively. Spin-coating the active material between the two gratings completes the laser. The peaks in reflectivity of such gratings are matched to the fluorescence spectra of PBD, PBD doped with C490, and PBD doped with both C490 and DCMII, as evident from Fig. 2. We have used these active gain media together with the distributed Bragg reflector resonator to fabricate ultraviolet, blue and red lasers, as shown in Fig. 3.

The measurements reported above were all made with spun films. The film quality of vacuum-sublimed films is sometimes better than that of spun films. We now describe the characteristics of optical amplifiers in which the active materials is 2-napthyl-4,5-bis(4-methoxyphenyl)-1,3-oxazole (NAPOXA) doped with ~1% DCMII. These films are deposited by co-sublimation and combine two important properties: good film-forming ability and almost perfect overlap between the host emission and guest absorption spectra, as can be observed in Fig. 4. With this system thresholds for stimulated emission were as low as 85 W cm^{-2} (total power). The pump energy density for these measurements was held constant at 0.1–0.2 μJ cm^{-2}, and the length of the gain region was varied in the range 1–3 cm while the width of the gain region was 3–4 mm. We believe that this is the lowest threshold power density for an organic film reported to date and is due principally to the fact that the combined absorption and other losses of the NAPOXA host and the

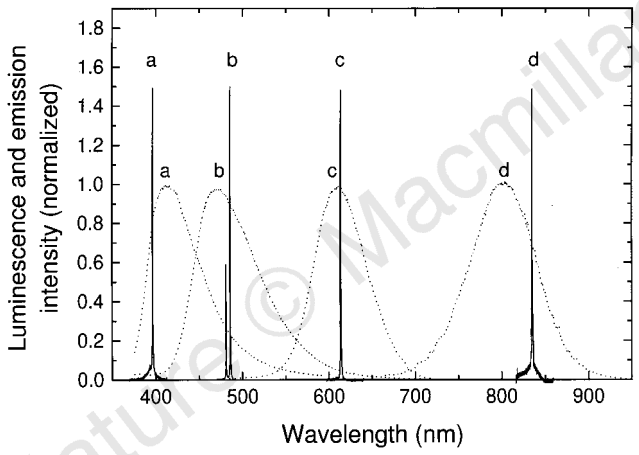

Figure 3 Laser emission spectra from devices made from four different active materials, and the spontaneous emission spectra of these materials. Solid lines, laser emission spectra; curve a, PBD; curve b, PBD + C490; curve c, PBD + C490 + DCMII; curve d, PBD + C490 + DCMII + LDS821. Dotted lines, spontaneous emission spectra for these active materials. The lasers producing emission spectra a, b and c used the same distributed Bragg reflector (DBR) resonator consisting of two 0.6-μm-pitch gratings etched in SiO_2 separated by a gain region 3–10 mm long. The third, fourth and fifth harmonics of the reflectivity of such DBR mirrors match the spontaneous emission spectra of c, b and a, respectively. The lasing threshold for pure films of PBD is quite high (10 kW cm^{-2}). The measured threshold power densities for the blue (b) and red (c) lasers are 1–1.5 kW cm^{-2} (total incident power density). The thresholds for the blue and red lasers are affected by losses in the SiO_2 cladding layer. As a result of these losses, the thresholds for observing ASE on these oxide-coated Si substrates (without a DBR) is ~10 kW cm^{-2}, much higher than the threshold for films on glass substrates. The laser thresholds can be further lowered by reducing optical losses in the SiO_2. For the laser d, a two-dimensional photonic bandgap based distributed feedback geometry is used. This is realized by using a SiO_2-coated Si substrate in which a square lattice of holes (with a circular cross-section and radius 0.15 μm) were etched. The depth of the holes is 10–30 nm and the lattice constant is 0.6 μm. The active material was spin-coated on such a patterned substrate to complete the device. The linewidths of the lasers a–d are resolution limited and are 0.2–0.3 nm.

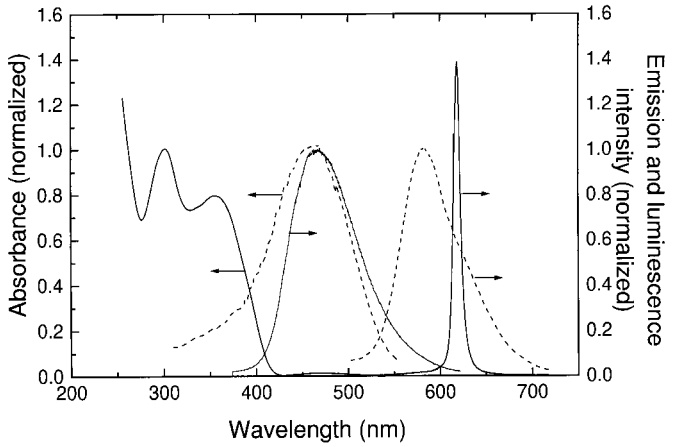

Figure 4 Absorbance and spontaneous emission spectra of the compounds used to make vacuum-sublimed films. Solid lines, 2-napthyl-4,5-bis(4-methoxyphenyl)-1,3-oxazole (NAPOXA); dashed lines, DCMII. Also shown is the stimulated emission spectrum from a film of NAPOXA doped with ~1% DCMII when excited at 250 kW cm^{-2}.

dye dopants at amplification wavelengths is small ($<1\,cm^{-1}$). The threshold power densities achieved ($<100\,W\,cm^{-2}$) compare very favourably with those reported for unpatterned films of conjugated polymers[6–8]. The low threshold powers in our system are a direct consequence of low loss at the emission wavelengths which allows the gain length to be increased to >2 cm.

Resonance energy transfer is fundamentally an electromagnetic interaction and the transfer rates can be influenced by strong microcavity effects. In high-*Q* cavities, this interaction between a donor and an acceptor is to be expected to stronger. This means that it may be possible to use an even smaller doping concentration and still achieve nearly complete transfer. This would have the potential to further lower absorption losses and thresholds and is a promising area for research.

The beneficial effects of energy transfer are not restricted to small organic molecules but also apply in the case of longer molecules such as oligomers and polymers. We have obtained low threshold power densities (for ASE detection) of $\sim 200\,W\,cm^{-2}$ for both polymer and oligomer emitters. The host material used is PBD and the emitters are a soluble derivative of polyphenylene vinylene) (10 wt%) and an oligomeric phenylene-vinylene (2 wt%). We measured a combined waveguide loss (due to effects such as absorption and scattering) of $0.6\,cm^{-1}$ in the case of the conjugated polymer emitter. Such low losses indicate that it is possible to use such materials in resonators with $Q > 10^5$, thereby accessing a regime where cavity electrodynamic effects can help to lower laser thresholds significantly. These results show the generality of our assertions that the absorption loss and threshold for stimulated emission is lowered, and the waveguiding properties improved, when the excitation is transferred down in energy in organic materials. □

Received 20 February; accepted 8 August 1997.

1. Schafer, F. P. in *Topics in Applied Physics: Dye Lasers* 3rd edn (ed. Schafer, F. P.) Ch. 1 (Springer, Berlin, 1990).
2. Weber, H. P. & Ulrich, R. A thin film ring laser. *Appl. Phys. Lett.* **19,** 38–40 (1971).
3. Kogelnik, H. & Shank, C. V. Stimulated emission in a periodic structure. *Appl. Phys. Lett.* **18,** 152–154 (1971).
4. Kaminov, I. P., Weber, H. P. & Chandross, E. A. Poly(methyl methacrylate) dye laser with internal diffraction grating. *Appl. Phys. Lett.* **18,** 497–499 (1971).
5. Gonokami, M. *et al*. Polymer microdisc and microring lasers. *Opt. Lett.* **20,** 2093–2095 (1995).
6. Tessler, N., Denton, G. J. & Friend, R. H. Lasing from conjugated polymer microcavities. *Nature* **382,** 695–697 (1996).
7. Hide, F. *et al*. Semiconducting polymers: a new class of solid state laser materials. *Science* **273,** 1833–1836 (1996).
8. Frolov, S. V. *et al*. Cooperative emission in π-conjugated polymer thin films. *Phys. Rev. Lett.* **78,** 729–736 (1997).
9. Förster, T. Transfer mechanisms of electronic excitation. *Disc. Faraday Soc.* **27,** 7–17 (1959).
10. Van Der Meer, B. W., Coker, G. & Chen, S. Y. in *Resonance Energy Transfer* Ch. 2 (VCH, New York, 1994).

Acknowledgements. We thank A. Timko and O. Nalamasu for the gratings, and E. A. Chandross and H. E. Katz for comments.

Correspondence and requests for materials should be addressed to A.D. (e-mail: ananth@bell-labs.com).

A chiral spherical molecular assembly held together by 60 hydrogen bonds

Leonard R. MacGillivray and Jerry L. Atwood

Department of Chemistry, University of Missouri-Columbia, Columbia, Missouri 65211, USA

Spontaneous self-assembly processes that lead to discrete spherical molecular structures are common in nature. Spherical viruses[1] (such as hepatitis B) and fullerenes[2] are well-known examples in which non-covalent and covalent forces, respectively, direct the assembly of smaller subunits into larger superstructures. A common feature of these shell-like architectures is their ability to encapsulate neutral and/or charged guests whose size, shape and chemical exteriors complement those of the host's inner surface[3,4]. Their interiors can often be regarded as a new phase of matter[5], capable of controlling the flow of reactants, transients and products, and of catalysing reactions of both chemical and biological relevance. Such properties have inspired the recent emergence of monomolecular[5–7] and supramolecular dimeric molecular capsules[8,9], many of which have been based on the head-to-head alignment of bowl-shaped polyaromatic macrocycles such as calix[4]arenes[5,7,9]. But true structural mimicry of frameworks akin to viruses and fullerenes, which are based on the self-assembly of $n > 3$ subunits, and where surface curvature is supplied by edge sharing of regular polygons, has remained elusive. Here we present an example of such a system: a chiral spherical molecular assembly held together by 60 hydrogen bonds (1) **(Fig. 1). We demonstrate the ability of** 1**, which consists of six calix[4]resorcinarenes** 2 **and eight water molecules, to self-assemble and maintain its structure in apolar media and to encapsulate guest species within a well-defined cavity that possesses an internal volume of about 1,375 Å^3. Single crystal X-ray analysis shows that its topology resembles that of a spherical virus[1] and conforms to the structure of a snub cube, one of the 13 Archimedean solids[10].**

Our interest in **2** lies in its ability to function as a multiple hydrogen bond donor in the solid state[11]. During experiments aimed at co-crystallizing *C*-methylcalix[4]resorcinarene **2a** with hydrogen bond acceptors in aromatic solvents, we have discovered the ability of **2a** to self-assemble as a spherical hexamer, along with adventitious water molecules, to form **1a** (Fig. 1). Subsequent solution studies have revealed the ability of *C*-undecylcalix[4]-resorcinarene **2b** to maintain the structure of the spheroid in apolar organic solvents. We now report the synthesis, X-ray crystal structure and solution behaviour of **1**.

Addition of **2a** (0.015 g) to a boiling aliquot of nitrobenzene (5 ml) yielded light yellow cubic crystals **3** suitable for X-ray analysis after a period of ~2 weeks. The formulation of **3** was confirmed by single-crystal X-ray diffraction and ^{1}H NMR spectroscopy (see Supplementary Information).

A cross-sectional view of the X-ray crystal structure of **1a** is shown in Fig. 1a. The assembly consists of six molecules of **2a** and eight molecules of water that have assembled, by way of 60 O–H···O hydrogen bonds, to form a shell-like octahedral cubic spheroid. The calixarenes, each of which lies around a four-fold axis, point their hydroxy groups along the periphery of **1a** and form two hydrogen bonds to two neighbouring calixarenes (O1···O1′ 2.73(1) Å) whereas the water molecules, each of which lies around a three-fold axis, are embedded along the surface of **1a** such that they lie on the vertices of a cube (edge length 9.00 Å) and participate in three hydrogen bonds with three different calixarenes (O2···O3 2.73(1) Å). Notably, each calixarene also exhibits four intramolecular hydrogen bonds, one at each of its corners (O1···O2 2.64(1) Å), which impart stability to its bowl-like conformation. As a result, **1a** possesses 4-3-2 symmetry (Fig. 1b–d), ignoring all hydroxy hydrogen atoms, and a well-defined central cavity with a maximum diameter of 17.7 Å and an internal volume of ~1,375 Å^3 (Fig. 1e)[12]. Indeed, the cavity of **1a** is vast, being more than 4.5 times larger than the cavity of the largest molecular capsule reported to date (~300 Å^3)[8]. Interestingly, the calixarenes of **1a** are twisted by 23° with respect to the faces of the water 'cuboid' which, as a consequence, makes **1a** chiral.

A view depicting the solid-state packing of **1a** reveals that neighbouring spheroids fall on their four-fold axes and their methyl groups lie staggered owing to the twisting displayed by the macrocycles (Fig. 1f). This gives rise to an interpenetrating body-centred cubic lattice that exhibits interstices between **1a** that are occupied by disordered water molecules, each of which participates in two hydrogen bonds with two water molecules from adjacent